Inorganic Chemistry

Article

pubs.acs.org/IC

$LiCa_3As_2H$ and $Ca_{14}As_6X_7$ (X = C, H, N): Two New Arsenide Hydride Phases Grown from Ca/Li Metal Flux

Trevor V. Blankenship,[†] Xiaoping Wang,[‡] Christina Hoffmann,[‡] and Susan E. Latturner*[,†]

[†]Department of Chemistry and Biochemistry, Florida State University, Tallahassee, Florida 32306, United States

[‡]Chemical and Engineering Materials Division, Oak Ridge National Laboratory, Oak Ridge, Tennessee 37831, United States

Supporting Information

ABSTRACT: The reaction of arsenic with sources of light elements in a Ca/Li melt leads to the formation of two new arsenide hydride phases. The predominant phase $Ca_{14}As_6X_7$ (X = C^{4-}, N^{3-}, H^-) exhibits a new tetragonal structure type in the space group *P4/mbm* (*a* = 15.749(1) Å, *c* = 9.1062(9) Å, Z = 4, R1 = 0.0150). The minor phase $LiCa_3As_2H$ also has a new structure type in the orthorhombic space group *Pnma* (*a* = 11.4064(7) Å, *b* = 4.2702(3) Å, *c* = 11.8762(8)Å, Z = 4, R1 = 0.0135). Both phases feature hydride and arsenide anions separated by calcium cations. The red color of these compounds indicates they should be charge-balanced. DOS calculations on $LiCa_3As_2H$ confirm a band gap of 1.4 eV; UV−vis spectroscopy on $Ca_{14}As_6X_7$ shows a band gap of 1.6 eV. Single-crystal neutron diffraction studies were necessary to determine the mixed occupancy of carbon, nitrogen, and hydrogen anions on the six light-element sites in $Ca_{14}As_6X_7$; these data indicated an overall stoichiometry of $Ca_{14}As_6C_{0.445}N_{1.135}H_{4.915}$.

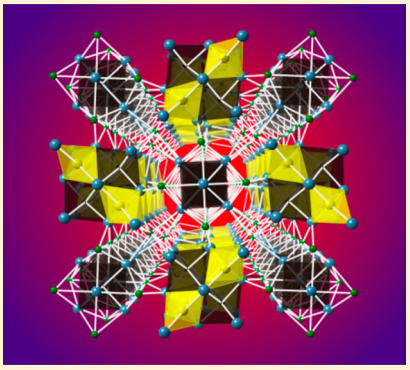

INTRODUCTION

Metal fluxes have proven to be excellent solvents for the synthesis and crystal growth of new intermetallic compounds.[1] The flux method eliminates the diffusion barrier present in traditional solid-state methods and enables crystals to be easily formed without lengthy annealing steps. We are investigating the use of mixed-metal fluxes which have a lowered melting point and will dissolve a larger variety of elements. Reactions in mixed fluxes have yielded new intermetallic phases, including $R_{3-\delta}FeAl_{4-x}Mg_xSi_2$ (R = Yb, Dy) and $R_5Mg_5Fe_4Al_{12}Si_8$ (R = Gd, Dy) grown from the Mg/Al eutectic,[2] $La_{21}Fe_8M_7C_{12}$ (M = Ge/Al, Sn, Sb, Te, Bi) and $LaNi_2Ru_2Al$ from the La/Ni eutectic,[3] and $Co_{7+x}Zn_{3-x}Sn_8$ from the Zn/Sn eutectic.[4]

The flux method is not a stoichiometric synthesis technique. The presence of excess flux metal can introduce a number of complications, including the possibility of contamination. This is often observed as unwanted incorporation of the flux element into products, whether as inclusions of flux droplets within bulk products or as substitutions of the flux element for others in the structure. An example of both of these phenomena is observed in the tin flux growth of $K_xBa_{1-x}Fe_2As_2$.[5,6] The crystals contain tin occlusions (evidenced by observation of the superconducting transition of tin) as well as some tin substitution on barium sites. Another contamination problem occurs when the flux metal(s) themselves are impure; since the flux is used in such a large excess, these contaminants can be present in significant amounts. This is particularly true for reactive metals such as alkaline-earth metals, which are known to be susceptible to hydride contamination and often have significant oxide coating. Inadvertent hydride contamination from alkaline-earth-metal reactants has been responsible for the discovery of phases such as $LiCa_2C_3H$, $Ba_{21}Ge_2O_5H_{24}$, and Ba_5Sb_3H.[7−9]

We are exploring the use of calcium/lithium melts as synthesis media. Ca/Li mixtures with 50 mol % lithium or greater have melting points below 300 °C and will dissolve most main-group elements and many binary hydrides, including CaH_2. Reactions such as Ca/Li/CaH_2/M (M = main-group metalloid) lead to crystal growth of complex hydride phases such as $LiCa_2C_3H$ and $LiCa_7Ge_3H_3$.[7,10] These compounds feature main-group and hydride anions surrounded by Ca^{2+} and/or Li^+ cations and are usually charge-balanced; they fall under the classification of Zintl phase hydrides. Zintl phases are typically comprised of electropositive metals (from groups 1 or 2) combined with main-group p-block metals or metalloids, yielding charge-balanced narrow band gap semiconductors. Zintl phase structures feature metal cations surrounding p-block element anions which can range from monoatomic (Sn^{4-} in $Ca_{11}Sn_3C_8$) to clusters (Sn_4^{4-} in Na_4Sn_4) to networks (K_8Sn_{44}); the p-block element accepts electrons and/or forms bonds to satisfy the octet rule.[11,12] Zintl phase hydrides contain both p-block anions and hydride anions, both surrounded by cations, and are exemplified by compounds such as Ca_3SnH_2 ($(Ca^{2+})_3(Sn^{4-})(H^-)_2$) and Ca_5Sb_3H ($(Ca^{2+})_5(Sb^{3-})_3(H^-)$).[13,14]

The Zintl phase hydride phases we have isolated from Ca/Li/CaH_2/M (M = C, Si, Ge, Sn) reactions have all been small band gap semiconductors. Extending this exploration to the more electronegative M = arsenic has led to formation of two

Received: July 17, 2014
Published: September 15, 2014

   dx.doi.org/10.1021/ic501722d | *Inorg. Chem.* 2014, 53, 10620−10626

Table 1. Crystallographic Data and Collection Parameters for Arsenide Hydride Phases

		$Ca_{14}As_6C_{0.445}N_{1.135}H_{4.915}$	
	$LiCa_3As_2H$	X-ray data	neutron data
formula wt	278.03	1037.35	1037.35
cryst syst	orthorhombic	tetragonal	tetragonal
space group	*Pnma*	*P*4/*mbm*	*P*4/*mbm*
a (Å)	11.4064(7)	15.7493(15)	15.7027(2)
b (Å)	4.2702(3)		
c (Å)	11.8762(8)	9.1062(9)	9.1043(2)
Z	4	4	4
V (Å^3)	578.46(7)	2258.7(4)	2244.89(6)
calcd density (g/cm^3)	3.192	3.049	3.068
index ranges	$-15 \le h \le 14$, $-5 \le k \le 5$, $-15 \le l \le 15$	$-20 \le h \le 19$, $-19 \le k \le 20$, $-12 \le l \le 11$	$-24 \le h \le 25$, $-25 \le k \le 26$, $-14 \le l \le 14$
collection temp (K)	200	200	100
no. of rflns collected	6015	25411	7364
no. of unique data/params	783/41	1530/71	1330/88
μ (mm^{-1})[a]	14.05	11.94	$(0.0333 + 0.0367) \times \lambda$
R1/wR2[b]	0.0135/0.0321	0.0165/0.0419	0.0541/0.0927
R1/wR2 (all data)	0.0145/0.0326	0.0170/0.0421	0.0547/0.0930
residual peak/hole (e Å^{-3})	0.38/−0.60	3.99/−0.48	1.02/−1.08[c]

[a]The neutron linear absorption coefficient is wavelength dependent, and it is calculated as $\mu = 0.0333 + 0.0367\lambda$ mm^{-1}. [b]$R1 = \sum||F_o| - |F_c||/\sum|F_o|$; $wR2 = [\sum[w(F_o^2 - F_c^2)^2]/\sum[w(F_o^2)^2]]^{1/2}$. [c]In units of fm Å^{-3}.

Table 2. Atomic Positions and Site Occupancies for $Ca_{14}As_6C_{0.445}N_{1.135}H_{4.915}$ from Single-Crystal Neutron Diffraction Data

	site	*x*	*y*	*z*	occ[a]	U_{eq}[b]
As(1)	4*g*	0.2844(1)	0.2155(1)	0		0.0043(3)
As(2)	4*h*	0.2364(1)	0.2636(1)	1/2		0.0040(3)
As(3)	16*l*	0.1979(1)	−0.0081(1)	0.2442(1)		0.0055(1)
Ca(1)	4*f*	1/2	0	0.3198(3)		0.0037(4)
Ca(2)	8*k*	0.3423(1)	0.1577(1)	0.3059(2)		0.0075(3)
Ca(3)	8*j*	0.0313(1)	0.3129(1)	1/2		0.0049(3)
Ca(4)	8*i*	0.3216(1)	0.0193(1)	0		0.0059(3)
Ca(5)	8*k*	0.1834(1)	0.3166(1)	−0.2100(2)		0.0074(3)
Ca(6)	4*e*	0	0	0.2512(3)		0.0058(4)
Ca(7)	8*i*	0.1211(1)	0.1137(1)	0		0.0096(4)
Ca(8)	8*j*	0.1188(1)	0.1089(1)	1/2		0.0086(4)
X(1)	4*h*	0.4162(1)	0.0838(1)	1/2	100% N	0.0042(2)
X(2)	2*b*	0	0	1/2	89(2)% C	0.0042(9)
X(3)	2*a*	0	0	0	27(2)% N, 43(2)% H	0.0041(2)
H(1)	4*g*	0.3830(3)	−0.1170(3)	0	70(3)% H	0.024(2)
H(2)	8*k*	0.0992(1)	0.4008(1)	−0.3387(4)		0.0203(6)
H(3)	8*k*	0.4255(1)	0.0745(1)	0.1470(4)		0.0192(6)

[a]All occupancies 100% except where noted. [b]U_{eq} is defined as one-third of the trace of the orthogonalized $\mathbf{U}_{ij}$ tensor.

new larger band gap phases, $LiCa_3As_2H$ and $Ca_{14}As_6X_7$ (X = C, H, N), with the latter incorporating contaminant atoms from the flux. Single-crystal neutron diffraction data were crucial in determination of the site occupation of these light atom impurities.

EXPERIMENTAL SECTION

Synthesis. Chunks of lithium (99.8% Strem), acetylene carbon black powder (99.5% Alfa Aesar), arsenic powder (99.9%, Alfa Aesar, stored under Ar), and calcium hydride powder (98%, Alfa Aesar) were used as received. Calcium shot (99.5% Alfa Aesar) was purified by heating in a steel tube under 10^{-5} Torr vacuum at 650 °C for 3 h. Heating was continued under 10^{-3} Torr for 12 h; the purified calcium was then cooled and stored under argon. This process decomposes any calcium hydride and calcium hydroxide present and removes the resulting gaseous hydrogen and water. Reactants and flux metals were placed in stainless steel crucibles (7.0 cm length/0.7 cm diameter) in a 7/7/0.7/1.4/0.7 mmol Ca/Li/As/C/CaH_2 ratio in an argon-filled glovebox. The crucibles were sealed by arc welding under argon and were placed in silica tubes which were flame-sealed under vacuum. The ampules were heated from room temperature to 1050 °C in 3 h and held there for 2 h. The reaction mixtures were cooled stepwise to 850 °C in 36 h, to 600 °C in 36 h, and then to 500 °C in 24 h. The reaction mixtures were held at 500 °C and then were removed from the furnace, inverted, and centrifuged for 2 min to separate the crystalline products from the Ca/Li melt. The solid product adheres to the side of the crucible. The steel crucibles were cut open in an argon-filled glovebox.

Additional syntheses were carried out upon discovering accidental nitride incorporation into the $Ca_{14}As_6X_7$ product. Ca_3N_2 (99% Cerac) was added to the reaction mixture to observe the effects on the reaction yield, which improved drastically and was optimized with a Ca/Li/As/C/CaH_2/Ca_3N_2 reactant ratio of 7/7/1.4/0.4/0.4/0.4 mmol. Reactants were loaded into stainless steel crucibles and prepared and heated using the previously described procedure.

dx.doi.org/10.1021/ic501722d | *Inorg. Chem.* 2014, 53, 10620−10626

Elemental Analysis. Elemental analyses were performed using a JEOL 5900 scanning electron microscope with energy dispersive spectroscopy (SEM-EDS) capabilities. Samples were affixed to an aluminum SEM stub using carbon tape and analyzed using a 30 kV accelerating voltage. The atomic ratios of calcium and arsenic could be determined with this method, but this method is not sensitive to the lighter elements. The average calcium/arsenic ratio determined from EDS was found to be 70%/30%, in agreement with the stoichiometry of the $Ca_{14}As_6X_7$ phase. The minority phase $LiCa_3As_2H$ has a similar Ca/As ratio and could not be distinguished from the predominant phase on the basis of EDS measurements. To analyze the lighter elements and confirm the presence of nitrogen indicated by neutron diffraction data (vide infra), a sample of $Ca_{14}As_6X_7$ was sent to Atlantic Microlabs for CHN analysis. This confirmed the presence of all three of these elements (0.37, 0.61, and 0.83% by weight, respectively).

Structural Characterization. Sample crystals were brought out of the glovebox under Paratone oil and were mounted in cryoloops. Single-crystal X-ray diffraction data were collected at 170 K under a stream of nitrogen using a Bruker APEX 2 CCD diffractometer with a Mo Kα radiation source. The data were integrated with the Bruker SAINT software and corrected for absorption effects using the multiscan method (SADABS).[15] Refinements of the structures were performed using the SHELXTL package.[16] The structure of $LiCa_3As_2H$ was solved in the orthorhombic space group *Pnma*; that of $Ca_{14}As_6X_7$ was solved in the tetragonal space group *P*4/*mbm*. The heavy-atom positions (Ca, As) in both structures were located using direct methods, and the light-element sites were refined by least-squares analysis of the electron density map and assigned using consideration of bond lengths and charge balancing. The lithium and hydride sites in $LiCa_3As_2H$ had stable occupancies and thermal parameters, with the hydride site refined isotropically. The presence of six light-element sites in the $Ca_{14}As_6X_7$ structure caused difficulties in structure determination using X-ray diffraction data, necessitating the use of neutron diffraction studies (see below). Four out of the six light-atom sites exhibited unstable occupancies and/or negative thermal parameters in the X-ray data refinement; their occupancies were therefore fixed to the values determined from the neutron diffraction study, and their isotropic thermal parameters were fixed to values exhibited by similar atoms in the structure. This causes some errors in the refinement such as a large maximum electron residual density on the 2*a* site (occupied by a mixture of N and H according to the neutron diffraction analysis). Details about the crystallographic data collection and parameters can be found in Tables 1 and 2 and in the Supporting Information. Powder X-ray diffraction studies were carried out on reaction products to observe relative yields and identify byproducts. In a glovebox, samples of solid products from each reaction were ground into powder and placed in an airtight sample holder to prevent oxidation. PXRD data were collected using a PANalytical X'Pert Pro X-ray powder diffractometer with a Cu Kα radiation source.

Due to the presence of six light-element sites and the possibility of mixed occupancy, single-crystal neutron diffraction data were collected on a crystal of $Ca_{14}As_6X_7$ using the TOPAZ instrument at Oak Ridge National Laboratory.[17] In a glovebox, the crystal was coated in Krytox grease and adhered to a Kapton tube on a sample pin with a magnetic base. This was attached to the goniometer head inside the TOPAZ sample chamber. The crystal was cooled to 100 K under a stream of nitrogen. Data were collected using 15 crystal orientations optimized with CrystalPlan software for an estimated 98% coverage of symmetry-equivalent reflections of the tetragonal cell.[18] Each orientation was measured for approximately 4.5 h. The integrated raw Bragg intensities were obtained using the 3D ellipsoidal *Q*-space integration method in Mantid.[17] Data reduction including neutron TOF spectrum, detector efficiency, and absorption corrections was carried out with the ANVRED2 program.[19] The reduced data were exported to GSAS format, and the structure was refined using the GSAS program suite.[20] Refinement parameters were the structure parameters, wavelength-dependent detector scaling, and extinction parameters. The extinction-corrected data were converted to the SHELX HKLF4 format in WinGX and refined to convergence.[21,22] The final *R* factors reduced to R1 = 0.0547 and wR2 = 0.0930 for 7364 reflections after removing 179 outlier reflections with a maximum $|F_o^2 - F_c^2|/\sigma(F_o^2) = 5\sigma$ cutoff (see Table 1).

Electronic Structure Calculations. Density of states calculations were carried out on $LiCa_3As_2H$ using the Stuttgart TB-LMTO-ASA software package.[23] The structural model for this phase was based on the unit cell dimensions and atomic coordinates derived from single-crystal X-ray diffraction data. Empty spheres were added by the program where appropriate to fill the unit cell volume. An $18 \times 6 \times 6$ κ-point mesh was used and integrated using the tetrahedron method. The basis sets consisted of 4s/4p/4d for As, 4s/4p/3d for Ca, 2s for Li, and 1s/2p/3d for H. The As 4d, Ca 4p, Li 2p/3d, and H 2p/3d orbitals were downfolded. Similar calculations were not carried out on $Ca_{14}As_6X_7$ because of the disorder in the structure; the presence of several mixed-occupancy sites would require an extremely large supercell as an ordered model.

UV/Vis Spectroscopy. A sample of $Ca_{14}As_6X_7$ was ground under argon and loaded into an airtight holder which was placed into a PerkinElmer Lambda 900 spectrometer with a Labsphere PELA-1000 integration sphere. The spectra were taken from 300 to 1200 nm with a slit width of 2.0 nm. Reflectance data were converted to absorption using the Kubelka–Munk equation. The absorbance edge is observed at 780 nm from the linear extrapolation. Similar measurements could not be carried out on the minority phase $LiCa_3As_2H$ due to the small quantity available.

RESULTS AND DISCUSSION

Synthesis and Reactivity. Reactions of arsenic with light-element (X = H, C, N) sources in a Ca/Li flux leads to the formation of two new arsenide hydride phases, $Ca_{14}As_6X_7$ and $LiCa_3As_2H$, as well as traces of LiCaAs, which is an analogue of the recently reported LiSrAs (with the TiNiSi structure type).[24] Both of the title phases form as dark red faceted crystals which are air-sensitive and must be handled under an inert atmosphere. Preparing each compound in isolation is challenging because the carbide-containing phase, $Ca_{14}As_6X_7$, can form without adding C to the reaction by leaching carbon from the steel crucible. Deliberate addition of higher amounts of carbon reactant favors the carbide. This phase was also found to have incorporated adventitious nitride; when a nitride source was deliberately added (as Ca_3N_2 reactant), the yield increased to about 50% on the basis of arsenic. The $LiCa_3As_2H$ phase is present as a small minority phase that is usually less than 10% of the total product. A powder X-ray diffraction pattern of the solid product of a reaction of (Ca/Li)/As/C/CaH_2 in a 10/10/1/2/1 mmol ratio indicates the presence of both phases and a small amount of LiCaAs byproduct (Supporting Information, Figure S1).

Structure and Properties of $LiCa_3As_2H$. $LiCa_3As_2H$ forms with a new structure type in the orthorhombic space group *Pnma*. Figure 1 displays the structure, highlighting the connectivity of the arsenide-centered clusters (Figure 1a) or the hydride-centered clusters (Figure 1b). Local coordination environments are shown in Figure 2. The strongly reducing flux converts the arsenic reactant to monatomic arsenide anions. The As(1) site is coordinated by seven Ca cations and two Li cations, forming a capped-square-antiprismatic As@Ca_7Li_2 cluster which is distorted by the short As–Li bond lengths (2.535(3)Å) in comparison to the much longer As–Ca bonds (2.9691(5)–3.2364(4)Å; see Table 3). The As(2) site is coordinated to seven Ca atoms and one Li atom in a bicapped-trigonal-prismatic As@Ca_7Li unit with the Li atom on one of the caps (As–Li bond 2.573(5) Å and As–Ca bonds 3.0327(4)–3.1222(4)Å). These As@Ca_7Li_2 and As@Ca_7Li clusters share edges and faces to form a network that defines

dx.doi.org/10.1021/ic501722d | *Inorg. Chem.* 2014, 53, 10620–10626

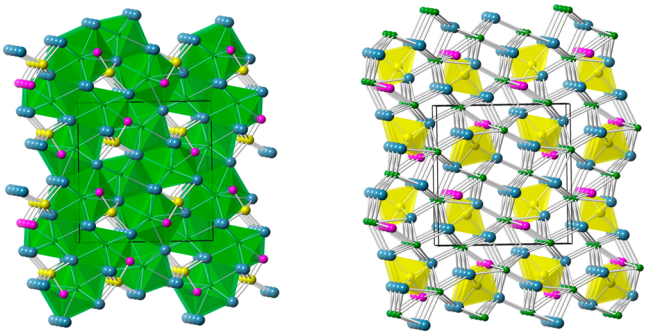

Figure 1. Orthorhombic structure of $LiCa_3As_2H$, viewed down the *b* axis, with different anion coordination polyhedra highlighted: (left) connectivity of arsenic-centered polyhedra (green); (right) connectivity of corner-sharing hydride-centered trigonal bipyramids (yellow). Blue and magenta spheres are calcium and lithium cations, respectively.

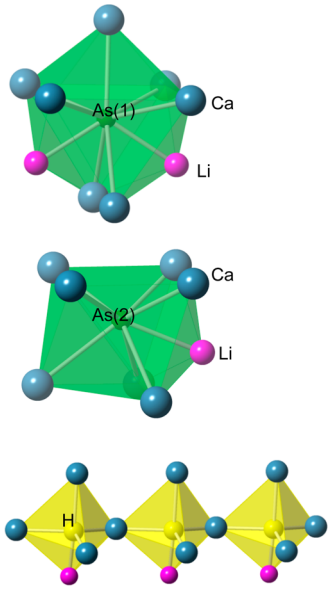

Figure 2. Coordination environments of anions in $LiCa_3As_2H$.

Table 3. Bond Lengths (Å) in Arsenide Hydride Phases

bond	
$LiCa_3As_2H$	
As(1)−Ca	2.9691(5)−3.2364(4)
As(1)−Li	2.535(3)
As(2)−Ca	3.0327(4)−3.1222(4)
As(2)−Li	2.573(5)
H(1)−Ca	2.302(1)−2.408(1)
H(1)−Li	2.070(3)
$Ca_{14}As_6X_7$	
As(1)−Ca	2.948(2)−3.137(2)
As(2)−Ca	2.891(2)−3.314(2)
As(3)−Ca	2.970(2)−3.498(1)
H(1)−Ca	2.348(6)−2.414(4)
H(2)−Ca	2.206(3)−2.280(3)
H(3)−Ca	2.281(3)−2.348(3)
X(1)−Ca	2.412(2)−2.481(2)
X(2)−Ca	2.265(3)−2.530(2)
X(3)−Ca	2.287(3)−2.608(2)

channels containing the hydride anions. The bond distances compare well to those reported for Li_3As (Li−As distance 2.57 Å) and Ca_5As_3 (Ca−As distances 2.90−3.13 Å).[25,26]

The hydride site is coordinated by four Ca cations and one Li cation, forming trigonal-bipyramidal $H@Ca_4Li$ clusters. These units share equatorial corners to form a chain running along the *b* axis. The H−Li bonds (2.070(3) Å) are axial and all point in the same direction in the chain. While each individual chain is polar, the symmetry equivalents are aligned in opposing directions, so that the net dipole is canceled. The Ca−H bond lengths range from 2.302(1) to 2.408(1)Å. These bond lengths are consistent with those seen in phases such as $BaLiH_3$ (Li−H distance 2.01 Å) and CaH_2 (Ca−H distances 2.27−2.65 Å).[7,27] An interesting point of comparison is $LiCa_2C_3H$, which is also grown from a Ca/Li flux. It features chains of corner-sharing $H@Li_2Ca_4$ units, with the hydride coordinated by both Ca (Ca−H = 2.502 Å) and Li (Li−H = 1.876 Å) ions in an octahedral arrangement.[7]

$LiCa_3As_2H$ is a complex salt which can be charge-balanced as $(Li^+)(Ca^{2+})_3(As^{3-})_2(H^-)$. Density of states (DOS) data are shown in Figure 3. These calculations indicate a band gap of 1.4

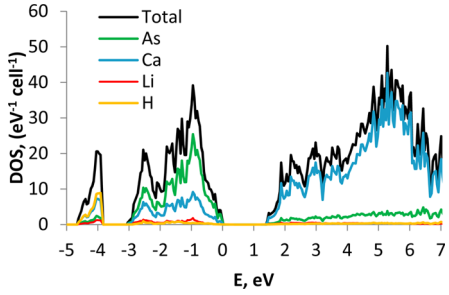

Figure 3. Calculated total and partial density of states data for $LiCa_3As_2H$.

eV, in agreement with the red color of the crystals. The binary salt Ca_3As_2 is also reported to have a reddish brown coloration.[28] The arsenic states of $LiCa_3As_2H$ make the dominant contributions to broad bands at and just below E_F (from 0 to −3 eV); calcium states are dominant above the band gap. The hydride states are localized well below E_F, between −4 and −5 eV. This is comparable to the calculated DOS for other Zintl phase hydrides; the hydride states in Ca_3SnH_2, $LiCa_2C_3H$, and $LiCa_7Ge_3H_3$ are also found 4 eV below the Fermi level.[7,10,13] These Zintl hydrides have band gaps significantly smaller (all below 0.5 eV) than those of the arsenides reported here. In these phases, the band gap is determined by the relative energies of the metalloid anion states which comprise the valence band and the calcium states which make up the conduction band. The greater electronegativity of arsenic leads to more stabilized valence bands and a larger band gap.

Structure of $Ca_{14}As_6X_7$ (X = C, H, N). $Ca_{14}As_6X_7$ also exhibits a new structure type, in the tetragonal space group *P*4/*mbm*, shown in Figure 4. It is composed of a network of edge- and face-sharing $As@Ca_8$ and $As@Ca_9$ clusters (shown in Figure 4a) interspersed with $X@Ca_6$ octahedra and $X@Ca_4$ tetrahedra which are linked into chains running along the *c* axis (Figure 4b). Of the three unique arsenide sites, two can be described as being surrounded by a snub disphenoid coordination of eight calcium cations, forming $As@Ca_8$ units. The other arsenide site has nine neighboring calcium sites, creating a monocapped-square-antiprismatic $As@Ca_9$ unit

dx.doi.org/10.1021/ic501722d | *Inorg. Chem.* 2014, 53, 10620−10626

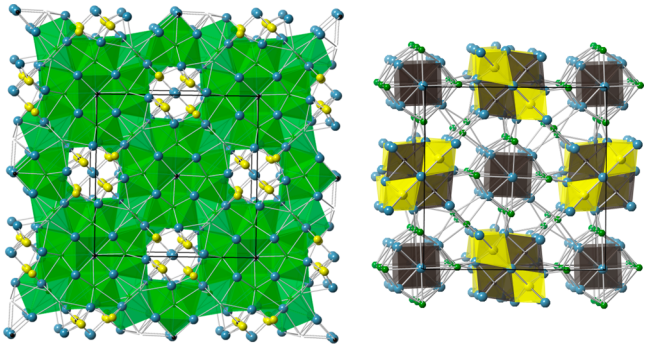

Figure 4. Tetragonal structure of $Ca_{14}As_6C_{0.445}N_{1.135}H_{4.915}$, viewed down the *c* axis, with different anion coordination polyhedra highlighted: (left) connectivity of arsenic-centered polyhedra (green); (right) connectivity of corner- and edge-sharing polyhedra centered by light atoms, with $H@Ca_4$ tetrahedra (yellow) and $X@Ca_6$ octahedra (black; X = C, H, N). Calcium cations are represented by blue spheres.

(Figure 5). The Ca–As bond distances in $Ca_{14}As_6X_7$ range from 2.891(2) to 3.498(1) Å. The longest bond, 3.498(1) Å, is

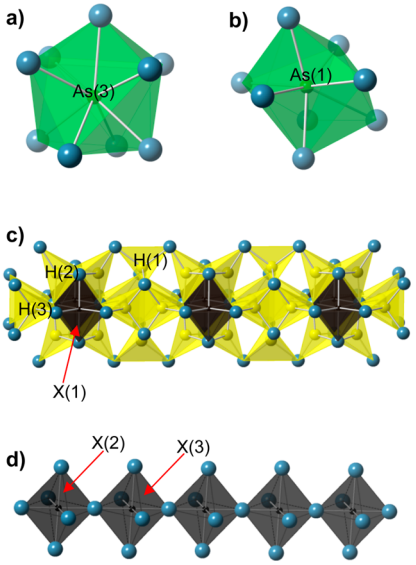

Figure 5. Local coordination environments for anions in $Ca_{14}As_6C_{0.445}N_{1.135}H_{4.915}$: (a) monocapped-square-prismatic coordination of As(3) by calcium cations; (b) snub disphenoid coordination of As(1) (similar coordination is found for As(2)); (c) chain of linked $H@Ca_4$ (yellow) and $X(1)@Ca_6$ (black) polyhedra; (d) chain of linked $X(2)@Ca_6$ and $X(3)@Ca_6$ polyhedra.

the As(3)–Ca(2) bond; this is considerably longer than the next longest Ca–As bond of 3.339(1) Å. This range of Ca–As bonds is larger than that observed for $LiCa_3As_2H$ (see Table 3) but is not unusual in comparison to other phases with arsenic sites coordinated by eight or more calcium atoms. The binary phase Ca_2As has arsenic coordinated by eight Ca atoms in a square antiprism with bond distances ranging from 3.00 to 3.32 Å, and the superconducting phase $Ca_{10}(Pt_3As_8)(FeAs_2)_5$ features Ca–As bonds ranging from 2.957 to 3.387 Å.[29,30] $Ca_{14}MnAs_{11}$ features 10-coordinate As with Ca–As bond lengths ranging from 2.895 to 3.562 Å.[31]

The $Ca_{14}As_6X_7$ structure has six unique light-atom positions (see Table 2). Three of these sites are tetrahedrally coordinated by calcium cations; occupancy refinements and bond lengths indicate these are most likely hydride sites (Ca–H distances in the range 2.206(3)–2.414(4)Å). These $H@Ca_4$ tetrahedra share corners and edges to form tubes running in the *c*-axis direction, surrounded by the calcium arsenide network. Also contained within these calcium hydride tubes is another light-atom site, X(1), coordinated by six calcium cations. The occupancy and bond lengths (in a small range of 2.412(2)–2.481(2) Å) suggest that this site is occupied by either carbon or a similar light element: X(1) = C, N. Each of these $X(1)@Ca_6$ units share edges with a symmetry equivalent and also share edges with $H@Ca_4$ units.

The two remaining light-atom sites, X(2) (on special position 2*b* at (0,0,1/2)) and X(3) (on special position 2*a*, at the origin of the unit cell), are also octahedrally coordinated by six calcium cations; these $X@Ca_6$ units share opposing corners to form a chain running along the *c* axis of the unit cell. Both of these octahedra are compressed along this axis; the X–Ca bonds to the axial (shared) corners are 2.265(3) or 2.287(3) Å, while the four equatorial X–Ca bonds are longer in each case (2.530(2) or 2.608(2) Å). This chain is surrounded by $As@Ca_9$ capped-square-antiprismatic clusters.

If the tetrahedrally coordinated light atoms are assigned as hydrides and the octahedrally coordinated light atom positions as carbides, full occupancy of all anionic sites would lead to a stoichiometry of $Ca_{14}As_6C_2H_5$ (Z = 4). This is not charge-balanced; $(Ca^{2+})_{14}(As^{3-})_6(C^{4-})_2(H^-)_5$ has a net negative charge. However, semiconducting charge-balanced behavior is indicated by the red coloration of the compound and the charge-balanced nature (and similar red color) of the coproduct $LiCa_3As_2H$. An absorption edge at 780 nm (corresponding to a band gap energy of 1.6 eV) can also be seen in the UV–vis reflectance spectrum collected on a sample of $Ca_{14}As_6X_7$ (see Figure 6). Partial occupancy of the arsenic sites was not

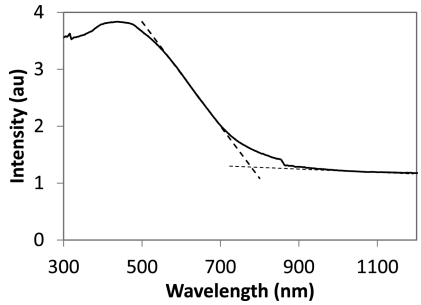

Figure 6. Absorbance spectrum of $Ca_{14}As_6X_7$ (X = C, H, N) from diffuse reflectance data.

indicated in the crystallographic data refinement. Partial or mixed occupancy on the carbide and hydride sites is therefore mandated, but occupancies of light elements are difficult to analyze from single-crystal X-ray diffraction data due to their low X-ray scattering factors. However, the neutron scattering lengths of carbon, hydrogen, and nitrogen are significantly different enough (6.6460, −3.7390, and 9.36 fm, respectively) to enable refinement of mixed or partial occupancies of these sites.[32] The single-crystal neutron diffraction data were analyzed using the constraints that all calcium and arsenic sites were fully occupied (as indicated by SCXRD) and that the charges should balance (as indicated by the red color of the crystals).

Of the six light element sites in the structure, the three that are tetrahedrally coordinated by Ca^{2+} ions (a 4*g* site and two 8*k* sites) had the smallest electron density peaks in the single-

dx.doi.org/10.1021/ic501722d | *Inorg. Chem.* 2014, 53, 10620–10626

crystal XRD refinement, indicative of hydride occupancy as mentioned above. This was supported by the neutron diffraction data; the two 8*k* sites could be refined as fully occupied by hydride with stable thermal parameters. The 4*g* site, on the other hand, refined slightly less than fully occupied (70(3)% hydride occupancy).

Refinement of the three octahedrally coordinated light element sites (X(1), X(2), and X(3) on 4*h*, 2*b*, and 2*a* sites, respectively) proved more complicated. These were originally assigned as carbon in the refinement of the SCXRD data; when the occupancy was allowed to refine, X(1) refined as over 100% occupied, X(2) as close to 100% occupied, and X(3) as below 100% occupied. However, it was immediately evident from the neutron diffraction data that the 4*h* site could not be occupied by carbon, as it had a much *larger* neutron scattering factor. This is also clearly distinct from the negative scattering factor of hydrogen; occupancy by oxygen is also precluded, since its neutron scattering factor of 5.803 fm is lower than that of carbon. The data clearly indicate occupancy by nitrogen, with the site refining as 100% occupied. These N(1)@Ca_6 octahedra are linked to one symmetry-equivalent and six surrounding H@Ca_4 tetrahedra by edge sharing, forming the chain depicted in Figure 5c. The Ca−N bond lengths are in a small range of 2.412(2)−2.481(2)Å. Similar distances are seen in Ca_3AsN and Ca_3N_2, both of which feature N@Ca_6 octahedra with bond lengths of 2.39−2.42 and 2.41−2.48 Å, respectively.[33,34]

The other two light-element sites center X(2)@Ca_6 and X(3)@Ca_6 octahedra which share opposing corners to form a chain running along the *c* axis (Figure 5d). Refinement of the neutron diffraction data indicates that X(2) is 89(2)% occupied by carbon, in agreement with the X-ray refinement, which also supports carbon at this site. The X(3) site had a low neutron scattering factor; charge-balancing considerations were used to aid in assigning the site occupancy. With three hydride sites (and 70(3)% occupancy of the 4*g* site), one nitride site, and one carbon site with 89(2)% occupancy, an overall stoichiometry of $Ca_{14}As_6N_1C_{0.445}H_{4.7}(X(3))_{0.5-d}$ is indicated, allowing for the fact that the X(3) site may be partially occupied. The charge and occupancy of the anions on the X(3) site must contribute −0.52 to the overall formula to allow for charge balancing. Unfortunately there are a number of variables involved—the anion mixture and site occupancy—but it is likely that this site is possibly partially occupied by a mixture of N and H. This site was refined as containing a mixture of 27(2)% N and 43(2)% H. This produces a low overall neutron scattering factor as expected with stable thermal parameters for this site and would also yield an apparent occupancy in the X-ray refinement lower than that of carbide. The resulting overall stoichiometry of $Ca_{14}As_6C_{0.445}N_{1.135}H_{4.915}$ is very close to being charge balanced.

The presence of nitrogen in $Ca_{14}As_6X_7$ was confirmed by elemental analysis and by the fact that the yield was dramatically increased when a nitride source was deliberately added as a reactant. CHN analysis indicated a nitrogen mass percentage of 0.83%, slightly lower than the 1.53% expected from the refined stoichiometry. The acetylene carbon black used as a reactant was also analyzed by CHN analysis and contained no nitrogen; the source of nitrogen appears to be the flux metals. Both lithium and calcium are known to form surface nitrides, and the large quantity of these metals used could lead to significant amount of nitride present in the melt.

In the flux synthesis of $Ca_{14}As_6C_{0.445}N_{1.135}H_{4.915}$, the growing crystals may scavenge from the molten metal solution whatever small anions are needed to maintain charge neutrality. The Ca_6 octahedra are large enough to incorporate C^{4-}, N^{3-}, and H^-. Similar behavior likely occurs during the formation of other mixed anion phases such $LiCa_{11}Ge_3OH_x$ and $(Ca,Y)_2Si_4(N,C)_7$.[10,35] Another mixed anion compound, $Ba_{21}Ge_2O_5H_{24}$, provides an interesting case study.[8] While this phase does not feature O^{2-} and H^- mixing on one site, a structural analogue ($Sr_{21}Si_2O_5C_6$) can be synthesized by substituting the H^- anions for C^{4-} anions, with partial occupancy of the carbide anions to balance the charge.[36] In these alkaline-earth-rich phases, the AE_6 octahedra are of suitable size to incorporate different small anions (and mixtures of anions), as is also seen in $Ca_{14}As_6C_{0.445}N_{1.135}H_{4.915}$.

CONCLUSIONS

The ability of calcium/lithium melts to dissolve ionic hydrides and main-group metalloids makes them rich growth media for complex metal hydrides. The high reactivity of these flux metals does lead to the possibility of impurities being incorporated into products. The use of purified (distilled or dentritic) alkali metals and alkaline-earth metals is recommended to avoid accidental incorporation of oxide, nitride, and hydride anions. However, incorporation of several different monatomic anions leads to new compounds often characterized by high levels of structural complexity.

The electronic properties of these charge-balanced Zintl hydride phases are predominantly determined by the main-group metalloid, which makes the dominant contributions to the valence band at the Fermi level. Incorporation of group 14 elements leads to small band gap Zintl hydrides such as $LiCa_7Ge_3H_3$, Ca_3SnH_2, and $LiCa_2C_3H$.[7,10,13] The use of arsenic, from group 15, leads to the two arsenide hydrides studied in this work, which have significantly larger band gaps. Use of group 13 metals on the other side of the "Zintl border"[12] (such as indium) results in phases with complete closing of the gap, metallic subhydride phases such as $Ca_{54}In_{13}B_{4-x}H_{23+x}$, which are no longer charge-balanced.[37]

ASSOCIATED CONTENT

Supporting Information

A figure giving powder X-ray diffraction data of solid product of flux reactions and CIF files giving crystallographic data for both title phases. This material is available free of charge via the Internet at http://pubs.acs.org.

AUTHOR INFORMATION

Corresponding Author

*E-mail for S.E.L.: latturne@chem.fsu.edu.

Notes

The authors declare no competing financial interest.

ACKNOWLEDGMENTS

This research was supported by funding from the National Science Foundation (Division of Materials Research) through grant number DMR-11-06150 and by the FSU Department of Chemistry and Biochemistry. This research made use of the scanning electron microscope facilities of the FSU Physics Department. Neutron scattering measurements were carried out at the ORNL Spallation Neutron Source, which is sponsored by the Division of Scientific User Facilities, Office of Basic Energy Sciences, U.S. Department of Energy, under Contract No. DE-AC05-00OR22725 with UT-Battelle, LLC.

REFERENCES

(1) Kanatzidis, M. G.; Pöttgen, R.; Jeitschko, W. *Angew. Chem., Int. Ed.* **2005**, *44*, 6996−6702.
(2) (a) Ma, X.; Whalen, J. B.; Cao, H.; Latturner, S. E. *Chem. Mater.* **2013**, *25*, 3363−3372. (b) Ma, X.; Chen, B.; Latturner, S. E. *Inorg. Chem.* **2012**, *51*, 6089−6095.
(3) (a) Benbow, E. M.; Dalal, N.; Latturner, S. E. *J. Am. Chem. Soc.* **2009**, *131*, 3349−3354. (b) Zaikina, J. V.; Jo, Y. J.; Latturner, S. E. *Inorg. Chem.* **2010**, *49*, 2773−2781.
(4) Reynolds, P. C.; Stojanovic, M.; Latturner, S. E. *J. Solid State Chem.* **2011**, *184*, 1875−1881.
(5) Ni, N.; Bud'ko, S. L.; Kreyssig, A.; Nandi, S.; Rustan, G. E.; Goldman, A. I.; Gupta, S.; Corbett, J. D.; Kracher, A.; Canfield, P. C. *Phys. Rev. B* **2008**, *78*, 014507.
(6) Mathieu, J.; Latturner, S. E. *Chem. Commun.* **2009**, *33*, 4965−4967.
(7) Lang, D. A.; Zaikina, J. V.; Lovingood, D. D.; Gedris, T. E.; Latturner, S. E. *J. Am. Chem. Soc.* **2010**, *132*, 17532−17530.
(8) Huang, B. Q.; Corbett, J. D. *Inorg. Chem.* **1998**, *37*, 1892−1899.
(9) Leon-Escamilla, E. A.; Corbett, J. D. *J. Alloys Compd.* **1998**, *265*, 104.
(10) (a) Lang, D. A.; Latturner, S. E. *Eur. J. Inorg. Chem.* **2011**, *26*, 4006−4011. (b) Lang, D. A. *New materials grown from Ca/Li flux.* Masters thesis, Florida State University, 2011.
(11) Blankenship, T. V.; Lita, A.; Latturner, S. E. *Inorg. Chem.* **2012**, *51*, 13345−13350.
(12) Kauzlarich, S. M. *Chemistry, structure, and bonding of Zintl phases and ions*; VCH: New York, 1996.
(13) (a) Huang, B.; Corbett, J. D. *Inorg. Chem.* **1997**, *36*, 3730−3734. (B) Orgaz, E.; Aburto, A. *Int. J. Quantum Chem.* **2005**, *101*, 783−792.
(14) Häussermann, U. *Z. Kristallogr.* **2008**, *223*, 628−635.
(15) *SAINT, version 6.02a*; Bruker AXS Inc., Madison WI, 2000.
(16) Sheldrick, G. M. *SHELXTL NT/2000, version 6.1*; Bruker AXS Inc., Madison, WI, 2000.
(17) Schultz, A. J.; Jorgensen, M. R. V.; Wang, X.; Mikkelson, R. L.; Mikkelson, D. J.; Lynch, V. E.; Peterson, P. F.; Green, M. L.; Hoffmann, C. M. *J. Appl. Crystallogr.* **2014**, *47*, 915.
(18) Zikovsky, J.; Peterson, P. F.; Wang, X. P.; Frost, M.; Hoffmann, C. *J. Appl. Crystallogr.* **2011**, *44*, 418.
(19) Schultz, A. J.; Srinivasan, K.; Teller, R. G.; Williams, J. M.; Lukehart, C. M. *J. Am. Chem. Soc.* **1984**, *106*, 999.
(20) Larson, A. C.; Von Dreele, R. B. *General Structure Analysis System (GSAS)*; Los Alamos National Laboratory Report LAUR 86-748; Los Alamos National Laboratory, Los Alamos, NM, 2004.
(21) Sheldrick, G. M. *Acta Crystallogr., Sect. A* **2008**, *64*, 112.
(22) Farrugia, L. *J. Appl. Crystallogr.* **2012**, *45*, 849.
(23) (a) Jepsen, O.; Burkhardt, A.; Andersen, O. K. *The Program TB-LMTO-ASA, version 4.7*; Max-Planck-Institut für Festkörperforschung, Stuttgart, Germany, 2000. (b) Blöchl, P. E.; Jepsen, O.; Andersen, O. K. *Phys. Rev. B* **1994**, *49*, 16223−16233.
(24) Feng, X. J.; Prots, Y.; Schmidt, M. P.; Hoffmann, S.; Veremchuk, I.; Schnelle, W.; Burkhardt, U.; Zhao, J. T.; Grin, Y. *Inorg. Chem.* **2013**, *52*, 8971−8978.
(25) Von Benda, K.; Juza, R. *Z. Anorg. Allg. Chem.* **1969**, *371*, 172−192.
(26) Bruzzone, G.; Franceschi, E.; Merlo, F. *J. Less-Common Met.* **1978**, *60* (1), 59−63.
(27) Blaschkowski, B.; Kaller, M.; Schleid, T. *Z. Anorg. Allg. Chem.* **2006**, *632*, 2149−2149.
(28) Ropp, R. C. *Encyclopedia of the Alkaline Earth Compounds.* Elsevier: Oxford, U.K., 2013.
(29) Huetz, A.; Nagorsen, G. *Z. Metallkd.* **1974**, *65*, 618−618.
(30) Ni, N.; Allred, J. M.; Chan, B. C.; Cava, R. J. *Proc. Natl. Acad. Sci. U.S.A.* **2011**, *108*, E1019−E1026.
(31) Rehr, A.; Kuromoto, T. Y.; Kauzlarich, S. M.; del Castillo, J.; Webb, D. J. *Chem. Mater.* **1994**, *6*, 93−99.
(32) Sears, V. F. *Neutron News* **1992**, *3*, 26−37.
(33) Chern, M. Y.; DiSalvo, F. J.; Parise, J. B.; Goldstone, J. A. *J. Solid State Chem.* **1992**, *96*, 426−435.
(34) Reckeweg, O.; DiSalvo, F. J. *Z. Anorg. Allg. Chem.* **2001**, *627*, 371−377.
(35) Liddell, K.; Thompson, D. P.; Teat, S. J. *J. Eur. Ceram. Soc.* **2005**, *25*, 49−54.
(36) Knoth, M.; Rossler, U.; Eisenmann, B. *Z. Anorg. Allg. Chem.* **2005**, *631*, 1237−1240.
(37) Blankenship, T. V.; Chen, B.; Latturner, S. E. *Chem. Mater.* **2014**, *26*, 3202−3208.